PCCP

View Online
Dynamic Article Links

Cite this: *Phys. Chem. Chem. Phys.*, 2011, **13**, 7685–7691

www.rsc.org/pccp

PAPER

Joint photoelectron and theoretical study of $(Rh_mCo_n)^-$ (m = 1–5, n = 1–2) cluster anions and their neutral counterparts†

Haopeng Wang,[a] Yeon Jae Ko,[a] Lius G. García,[b] Prasenjit Sen,[c] Marcela R. Beltrán*[b] and Kit H. Bowen*[a]

Received 2nd September 2010, Accepted 2nd March 2011
DOI: 10.1039/c0cp01674h

Anion photoelectron spectroscopic experiments and calculations based on density functional theory have been used to investigate and uniquely identify the structural, electronic, and magnetic properties of both neutral and anionic (Rh_mCo_n) and $(Rh_mCo_n)^-$ (m = 1–5, n = 1–2) clusters, respectively. Negative ion photoelectron spectra are presented for electron binding energies up to 3.493 eV. The calculated electron affinities and vertical detachment energies are in good agreement with the measured values. Computational results for geometric structures and magnetic moments of both cluster anions and their neutrals are presented.

I. Introduction

For both scientific and technological reasons, interest in atomic clusters has grown in recent years. In particular, transition metal (TM) clusters have novel and highly size dependent electronic, chemical, optical, and magnetic properties at the nanometric scale,[1] reflecting the important role played by their structures. In some cases, a single size cluster is found to possess unexpected properties, such as multiple reaction rates[2–5] or multiple ionization potentials,[6,7] and these have been attributed to the presence of geometric isomers, each having its own properties. Combined experimental and computational investigations of the structures and properties of clusters support this interpretation.[8–11] The determination of the geometric structure of transition metal (TM) clusters is a vital step towards understanding cluster properties, such as catalytic and magnetic properties. Particularly interesting among TM clusters are those containing cobalt, since small cobalt clusters exhibit magnetic moments that are considerably larger than that of bulk cobalt. (Cobalt clusters preserve the atomic magnetic moment value of 2 μ_B per atom[12–16] up to clusters with diameters of $\sim$1.5 nm.) In general, the enhancement of magnetism in clusters can be qualitatively understood as a consequence of the reduction of local coordination number, which in turn results in a stronger localization of 3d electrons, and in a reduction of the effective d band width. Also, the size dependence of the interatomic distances, typically 20% smaller than those in bulk crystals, plays an important role in determining the ground state magnetic moments. Finally, finite size effects and reduced symmetry are also responsible for the magnetic anisotropy energies per atom found in TM clusters.

While many experimental and theoretical studies have already been carried out on homonuclear TM clusters, very few investigations have focused on mixed (alloy) clusters.[17] Heteronuclear clusters exhibit a much wider variety of magnetic behaviors due to more variables coming into play.[15,18–22] For example, recent experimental studies have shown that rhodium/cobalt nanoparticles exhibit enhanced average magnetizations per atom compared to macroscopic rhodium/cobalt alloys of similar compositions.[23] They are also expected to show larger magnetic anisotropies compared to pure 3d TM clusters due to the stronger spin orbit coupling at the 4d atoms.[13,24] Consequently, a comprehensive study of the properties of mixed 3d–4d TM clusters should be valuable.

Here, we report a negative ion photoelectron spectroscopy (PES) study combined with theoretical calculations done with density functional theory (DFT) using the generalized gradient approximation (GGA)[25–28] for exchange–correlation functional for the anionic and neutral clusters, $(Rh_mCo_n)^-$ and Rh_mCo_n (m = 1–5, n = 1–2), respectively. Previous computational work has examined magnetic and structural aspects of several rhodium/cobalt neutral clusters.[19,24,29] The present work incorporates an experimental (and its complementary computational) component by considering rhodium/cobalt anionic clusters, while at the same time providing a more complete picture of the geometries, electronic structure, and magnetic properties of both of these anionic and neutral rhodium/cobalt clusters.

[a] *Department of Chemistry, Johns Hopkins University, Baltimore, MD 21218, USA. E-mail: kbowen@jhu.edu*
[b] *Instituto de Investigaciones en Materiales, Universidad Nacional Autónoma de México, Cd. Universitaria, circuito exterior s/n A.P. 70-360, C.P. 04510, México DF. E-mail: mbeltran@servidor.unam.mx*
[c] *Harish-Chandra Research Institute, Chhatnag Road, Jhunsi, Allahabad 211019, India*

† This article was submitted following the 1st workshop on Energy Materials, organised by The Thomas Young Centre, and held on 7–9 September 2010 at University College London.

II. Methods

A Experimental

Negative ion photoelectron spectroscopy is conducted by crossing a beam of mass selected anions with a fixed-frequency photon beam and energy analyzing the resultant photo-detached electrons. The photodetachment process is governed by the energy conserving relationship, $h\nu = EBE + EKE$, where $h\nu$ is the photon energy, EBE is the electron binding energy, and EKE is the electron kinetic energy. Our apparatus has been described previously elsewhere.[30] Briefly, the apparatus consists of an ion source, a linear time-of-flight (TOF) mass spectrometer, a Nd:YAG (yttrium aluminium garnet) photo-detachment laser, and a magnetic bottle photoelectron spectrometer (MB-PES). The instrumental resolution of the MB-PES is ~35 meV at 1 eV EKE. The third harmonic (355 nm, 3.493 eV) of a Nd:YAG was used to photodetach the cluster anions of interest. Photoelectron spectra were calibrated against the well known atomic transitions of Cu^-.

Mixed rhodium-cobalt cluster anions were generated in a laser vaporization disk source. First, a cobalt disk was made by pressing pure cobalt powder under a pressure of ~170 MPa. Then a layer of rhodium powder was deposited on top of the cobalt disk, and pressed again under the same pressure of ~170 MPa. We then assured that the laser would vaporize both components, this particular procedure has been done to avoid diluting the Rh too much. This rhodium/cobalt disk was then ablated by a pulsed laser beam of 532 nm photons from a Nd:YAG laser. The plasma was cooled by supersonically expanding a plume of helium carrier gas issuing from a pulsed valve with a backing pressure of ~1 MPa. The negatively charged clusters were then extracted into our spectrometer for photoelectron spectroscopy studies.

B Computational

A structural optimization and frequency analysis has been performed on $(Rh_mCo_n)^-$ and Rh_mCo_n (m = 1–5, n = 1–2) clusters using density functional theory (DFT) calculations using generalized gradient approximation (GGA)[25] for the exchange–correlation functional. We present results for the Perdew Burke Ernzerhof (PBE)[31] GGA in this paper. Other exchange and correlation functionals have also been tested but not presented in this work. In order to perform the calculations we used double zeta plus valence polarization (DZVP) all-electron basis sets.[32] DZVP means that each atomic orbital is expressed as the sum of two Slater-type orbitals (STOs), (Z) zeta value accounts for how diffuse (large) the orbital is. As it takes too much effort to calculate a double-zeta for every orbital, instead, many scientists simplify matters by calculating a double-zeta only for the valence orbital. Since the inner-shell electrons aren't as vital to the calculation, they are described with a single Slater orbital. This method is called a split-valence basis set, and is written as DZV. Finally, (P) stands for polarization, to acknowledge and account for the fact that sometimes orbitals share qualities of 's' and 'p' orbitals or 'p' and 'd', *etc*., and not necessarily have characteristics of only one or the other. As atoms are brought close together, their charge distribution causes a polarization effect (the positive charge is drawn to one side while the negative charge is drawn to the other) which distorts the shape of the atomic orbitals. In this case, 's' orbitals begin to have a little of the 'p' flavor and 'p' orbitals begin to have a little of the 'd' flavor.

To locate different minima on the potential energy surface of the neutral, cationic and anionic clusters, a quasi-Newton method[33] with analytic energy gradients was used for the structure optimization. The convergence was based on the gradient and displacement vectors with a threshold of 10^{-4} a.u. The exchange–correlation potential was numerically integrated on an adaptive grid.[34] The grid accuracy was set to 10^{-6} in all calculations. The Coulomb energy was calculated by the variational fitting procedure previously described by Dunlap, Connolly and Sabin.[35,36] The auxiliary density was expanded in primitive Hermite Gaussian functions using the GEN-A2 auxiliary function set that contains s, p, d, f and g auxiliary functions, and adapts automatically to the chosen orbital basis set.[37] The exchange and correlation potential was calculated with the orbital density including zero point energy corrections. The convergence was based on the gradient and displacement vectors with a threshold of 10^{-5} a.u. For the vibrational analysis, the second derivatives were calculated by numerical differentiation (two-point finite difference) of the analytic energy gradients using a displacement of 0.002 a.u. from the optimized geometry for all $3N$ coordinates. The harmonic frequencies were obtained by diagonalizing the mass-weighted Cartesian force constant matrix. In the study of the cluster magnetic properties, only the atomic spin magnetic moments were computed, *i.e*. spin orbit interactions were not taken into account. While this is obviously an approximation, this may be justified on two grounds. Firstly, we are not interested in calculating the value of the magnetic anisotropy energy. Secondly, we are still able to identify the ground state structures of the clusters, as good agreement with experimental numbers for AEA shows. All calculations were performed using the density functional theory (DFT) deMon2k program.[38]

III. Results and discussion

In Fig. 1, we present the anion photoelectron spectra of Rh_mCo^- (m = 1–5) and $Rh_mCo_2^-$ (m = 1–2) clusters, each recorded with 355 nm photons. Peaks in the spectra are due to transitions from the ground electronic state of the anion to the ground and excited electronic and vibrational states of the resulting neutral species. In each of the photo-electron spectra, several transitions were observed. The EBE value in the onset (threshold) region of the lowest energy and the electronic transition (lowest EBE peak) in the spectrum give an estimate of the adiabatic detachment energy (ADE) of anion. The ADE is the energy difference between an anion and its corresponding neutral with the neutral relaxed into its nearest local minimum. In these cases, the ADE is also the adiabatic electron affinity (AEA) when both the anion and its corresponding neutral are in their ground states. The EBE value of the intensity maximum in the lowest EBE transition (peak) in the spectrum is the vertical detachment energy (VDE), which is defined as the

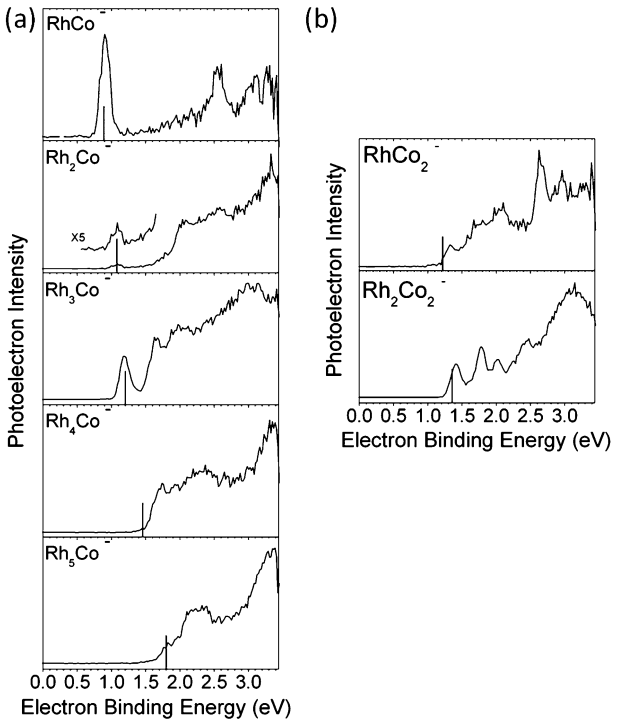

Fig. 1 Anion photoelectron spectra of (a) $(Rh_mCo)^-$ ($1 \leq m \leq 5$) and (b) $(Rh_mCo_2)^-$ ($m = 1, 2$) clusters recorded with 355 nm photons. The vertical solid sticks indicate the calculated adiabatic detachment energies (ADE).

energy difference between the anion and the neutral at the geometry of the anion. The ADE and VDE values, extracted from the experimental spectra, are listed in columns 2 and 3 of Table 1.

The ADE and VDE values of these species were also calculated in our DFT[38] calculations. The calculated ADE and VDE are listed in columns 4 and 5 of Table 1, respectively. The calculated ADEs are also indicated by the vertical bars in Fig. 1. Quantitatively, the experimental and computational results are in good agreement. For example, in the case of Rh_2Co_2, the EBE at the maximum of the most intense peak is 1.40 ± 0.05 eV, and the computed EBE value for the most prominent peak is 1.391 eV. These values are the experimental and computational measures of VDE. Additionally, the ADE is measured to be 1.23 ± 0.05 eV, which agrees with the calculated value of 1.356 eV.

Table 1 Experimental and calculated adiabatic electron affinities (AEA) and vertical detachment energies (VDE) for neutral and anionic Rh_mCo ($m = 1$–5) and Rh_mCo_2 ($m = 1$–2) clusters, respectively

	Experimental		Calculated	
Structure	ADE (eV)	VDE (eV)	ADE (eV)	VDE (eV)
RhCo	0.72	0.90	0.896	1.361
Rh_2Co	0.90	1.06	1.079	1.096
$RhCo_2$	1.16	1.32	1.222	1.314
Rh_3Co	1.02	1.18	1.206	1.358
Rh_2Co_2	1.20	1.40	1.357	1.389
Rh_4Co	1.44	1.70	1.469	1.810
Rh_5Co	1.63	1.80	1.620	1.690

The geometry of the ground state structures obtained for the neutral Rh_mCo_n ($m = 1$–5, $n = 1$–2) clusters is shown in Fig. 2. At the right hand side of each figure, (a) through (g), is plotted the charge density of the HOMO–LUMO Kohn–Sham molecular orbitals (MOs) , where light grey corresponds to regions with excess electrons and dark grey corresponds to electron deficit regions.

Fig. 3 Shows the anionic $(Rh_mCo_n)^{-1}$ ($m = 1$–5, $n = 1$–2) ground state clusters in a similar way as in Fig. 2. Each figure, (a) through (g), is followed by the charge density of the HOMO–LUMO Kohn–Sham molecular orbitals (MOs) at their right hand side. These structures are the result of an accurate determination of the lowest-energy points on the potential energy surface for these clusters. Isomers of different geometric forms, at each fixed stoichiometry, have been taken into consideration, followed by structures of fixed geometry that differ only in the distribution of the two types of atoms among the sites of the cluster. A reasonable set of starting geometries have been explored with all the possible nonequivalent sites of the cobalt atoms in the binary cluster. All the different possible configurations of the atomic spin magnetic moments (or multiplicities) for each geometry structure has been explored for both the anionic and the neutral systems.

As indicated above, all clusters were examined in detail using the DFT DeMon package.[38] Analyzing both figures at the same time, one can see small structural differences (varying bond distances) as the cluster goes from the anionic state towards the relaxed neutral configuration. For the charge density, notice the changes in the charge distribution upon ionization. These differences are reflected in the changing appearance in the PS spectra (shown in Fig. 1) and clearly it is reflected in Fig. 4, where we show the energy gaps between the highest occupied molecular orbital (HOMO) and the lowest unoccupied molecular orbital (LUMO) for Rh_mCo ($m = 1$–5) and Rh_mCo_2 ($m = 1$–2). It is interesting that the HOMO–LUMO (H–L) gaps alternate in value between the neutrals and their corresponding anions after $n = 2$. In Fig. 5 we show graphically the behavior of the magnetic moments for Rh_mCo ($m = 1$–5) and Rh_mCo_2 ($m = 1$–2) clusters, which were obtained by combining the experimental PS spectra and the computational results (shown in Table 2, columns 4 and 5).

This is achieved through the quantitative agreement between the calculated (VDEs), from the anion ground state with multiplicity M to neutral species (at the anion geometry) with multiplicity $M \pm 1$, with the experimental peaks. To extract this result we consider that the ionic cluster has an N number of unpaired spins and thus a magnetic moment of $N\mu_B$ and a spin multiplicity of $M = N + 1$ (as knowing the spin multiplicity, one knows the spin magnetic moment $2S + 1 = M$). As an electron is detached the neutral cluster can have a spin multiplicity of $M + 1$ or $M - 1$, depending upon whether the electron was removed from the minority or majority state. One can observe an alternating behavior between anions and neutral clusters as a result of modifications in the Fermi energy and band filling. The variations in the magnetic moment are related to the relative position of the unoccupied spin up or down orbital, and thus it is a signature of the nature of the LUMOs in the parent cluster.[39] Photoelectron spectroscopy is actually the most accurate

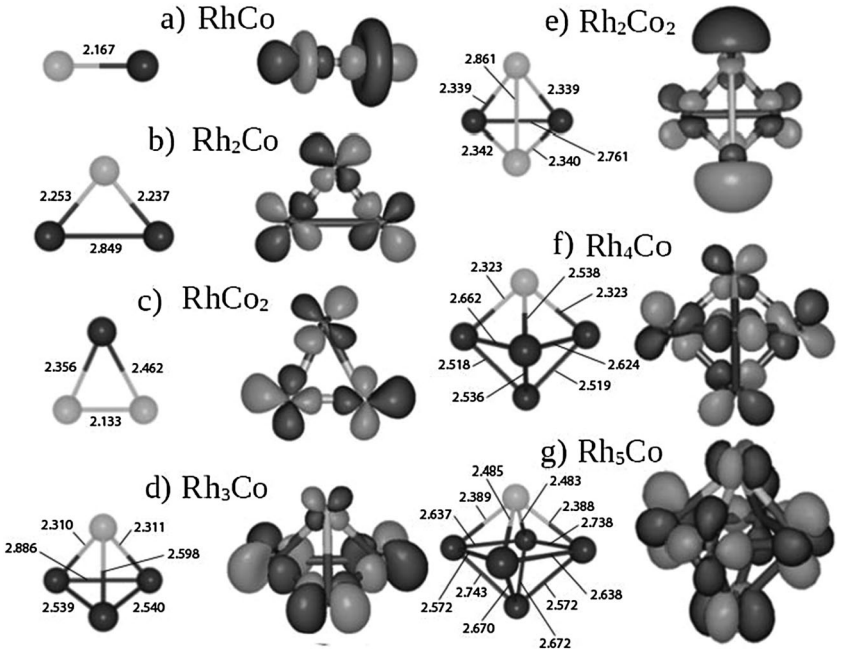

Fig. 2 Figures (a) through (g) show the geometry configurations of Rh_mCo ($1 \leq m \leq 5$) and Rh_mCo_2 ($m = 1, 2$) for neutral clusters shown on the left, followed by the electronic charge distribution of the HOMO–LUMO molecular orbitals on the right hand side.

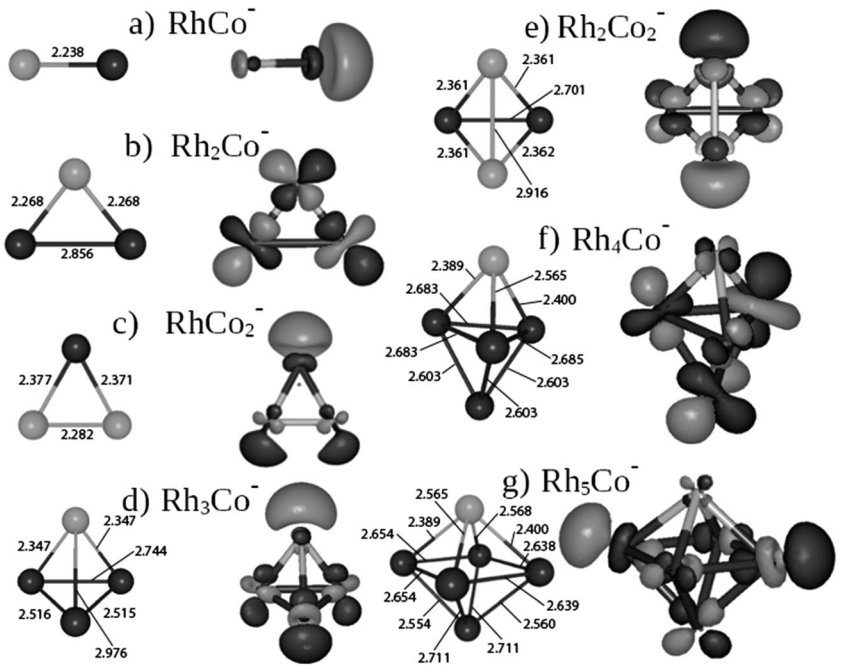

Fig. 3 Figures (a) through (g) show the geometry configurations of the $(Rh_mCo)^-$ ($1 \leq m \leq 5$) and $(Rh_mCo_2)^-$ ($m = 1, 2$) anionic clusters on the left side, followed by the electronic charge distribution of the HOMO–LUMO molecular orbitals to their right.

experimental method to provide information on the spin multiplicity and the ground state geometry when combined with theory. If the calculated energies agree with the experiment, quantitatively one can conclude that the multiplicity calculated by theory must be correct.[26,27] Nevertheless, several considerations and complications have to be considered. First of all, one must be aware that in some cases the ground state structure of the anion and the neutral can be different, resulting in the broadening of the spectra. In addition, transitions from the anion to the vibrational or electronic excited states of the neutral can occur, which will produce further structures in the experimental spectra and complicate the interpretation of the peaks. And also the fact that both neutrals and anions could possess isomers that are energetically nearly degenerate. Therefore, for a good interpretation of the PES spectra the theoretical counterpart must comprehend the calculations of

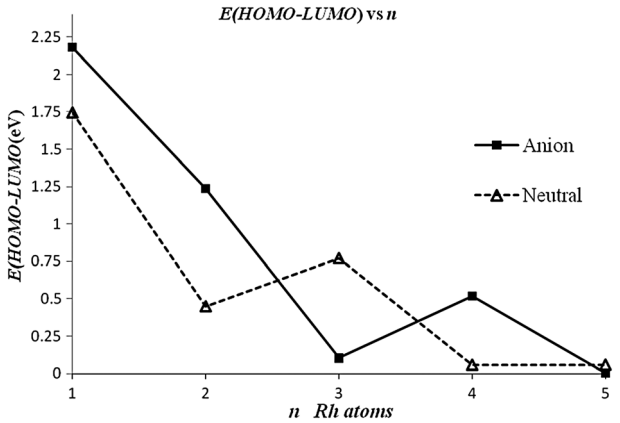

Fig. 4 Graphical illustration of the HOMO–LUMO gap behavior for the lowest energy isomers of neutral (open triangles) and anionic (solid squares) Rh_mCo ($1 \leq m \leq 5$) clusters.

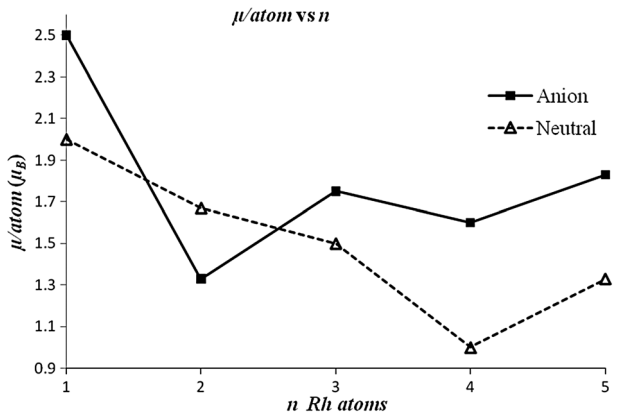

Fig. 5 Graphical illustration of the magnetic moments per atom of neutral (open triangles) and anionic (solid squares) Rh_mCo ($1 \leq m \leq 5$) clusters.

all allowed spin states and all possible isomeric forms for both neutral and the anionic configurations.

Notice that our calculated magnetic moments for some of the Rh_mCo_n clusters also agree with previous calculations done *via* different theoretical approaches for RhCo where a value of 2.00 μ_B per atom is obtained, which is similar to the value obtained by Dennler *et al.*[24] and Lv *et al.*[29] For Rh_2Co and $RhCo_2$, a value of 1.67 μ_B is obtained by us and by Dennler *et al.*[24] However, our calculated value for the Rh_2Co_2 is 2.0 μ_B, which, while agreeing with Dennler *et al.*'s result,[24] does not agree with Lv *et al.*'s[29] value of 1.50 μ_B at the same geometry.

In Table 2 we show the binding energy per atom in column 2; binding energy (E_b) of a cluster is defined as the energy gained in assembling the cluster from its isolated constituents atoms.

$$E_b = \sum_i E_i(\text{atom}) - E_T(\text{cluster})$$

where E_i(atom) is the energy of the ith isolated atom, and E_T(cluster) is the total energy of the cluster. In the case of our bimetallic clusters Rh_mCo_n, this quantity is calculated using the expression:

$$E_b = (mE_{Rh} + nE_{Co} - E_{RhmCon})/(m + n)$$

where, E_{RhmCon}, E_{Rh} and E_{Co} are the total energy of the bimetallic cluster, and the energies of an isolated Rh and Co atom, respectively. E_b can be used to establish the relative stability of clusters with different structures. Table 2 column 3 shows the adiabatic ionization potential, which involves the full minimization and search for minima of the positively charged clusters as a further reference. The magnetic moments found for all of the neutral structures are shown in Table 2 column 4, while column 5 shows the magnetic moments found for the anionic clusters. The largest magnetic moment per atom found is 2.5 μ_B for the $(RhCo)^-$ mixed dimer anion. Columns 6 and 7 show the numerical values of the HOMO–LUMO gaps for the neutral and the anionic clusters.

Finally, we calculated fundamental vibrational harmonic frequencies for all neutral clusters; the results are presented in Table 3. The fundamental vibrational harmonic frequencies for the negatively charged clusters are presented in Table 4. These values were used to guarantee that the structures obtained were actually local minima and not transitional states, and also to obtain the zero point energies which have been included in the results.

IV. Conclusion

In the present work we have performed a comprehensive study of the energetic, structural, electronic, and magnetic properties of both anionic and neutral $(Rh_mCo_n)^-$ and Rh_mCo_n (m = 1–5, n = 1–2) clusters, by using a synergistic approach which combined anion photoelectron spectroscopy and DFT based theoretical calculations. The total energy calculations quantitatively account for the photodetachment spectra and validates that the ground state structures of these clusters have

Table 2 Calculated binding energies per atom, adiabatic ionization potentials, magnetic moments and the HOMO–LUMO gaps for neutral and anionic Rh_mCo (m = 1–5) and Rh_mCo_2 (m = 1–2) clusters, respectively

			μ (μ_B)		HOMO–LUMO gap (eV)	
Structure	E_b/atom (eV)	AIP (eV)	Neutral	Anion	Neutral	Anion
RhCo	1.879	7.616	2.00	2.50	1.746	2.183
Rh_2Co	2.364	6.820	1.67	1.33	0.450	1.236
$RhCo_2$	2.211	6.329	1.67	2.00	0.753	0.029
Rh_3Co	2.760	6.390	1.50	1.75	0.772	0.103
Rh_2Co_2	2.731	6.100	2.00	1.75	0.330	0.283
Rh_4Co	2.984	6.324	1.00	2.00	0.058	0.518
Rh_5Co	3.823	5.896	1.33	1.83	0.059	0.003

Table 3 The calculated vibrational harmonic frequencies (cm^{-1}) for the lowest energy minima in neutral Rh_mCo ($1 \leq m \leq 5$) and Rh_mCo_2 ($m = 1, 2$) clusters

Rh_5Co	Rh_4Co	Rh_3Co	Rh_2Co	RhCo	$RhCo_2$	Rh_2Co_2
55	88	92	96	331	99	101
89	98	121	262	—	208	135
92	140	159	315	—	323	142
115	149	203	—	—	—	232
132	166	240	—	—	—	243
143	172	306	—	—	—	306
164	235	—	—	—	—	—
188	268	—	—	—	—	—
214	285	—	—	—	—	—
220	—	—	—	—	—	—
243	—	—	—	—	—	—
281	—	—	—	—	—	—

Table 4 Calculated vibrational harmonic frequencies (cm^{-1}) for the lowest energy minima in anionic Rh_mCo ($1 \leq m \leq 5$) and Rh_mCo_2 ($m = 1, 2$) clusters

Rh_5Co^-	Rh_4Co^-	Rh_3Co^-	Rh_2Co^-	$RhCo^-$	$RhCo_2^-$	$Rh_2Co_2^-$
77	103	79	104	285	78	90
85	105	114	240	—	180	134
90	131	153	307	—	286	183
107	132	205	—	—	—	215
113	161	215	—	—	—	238
133	167	284	—	—	—	298
154	168	—	—	—	—	—
184	225	—	—	—	—	—
207	273	—	—	—	—	—
221	—	—	—	—	—	—
231	—	—	—	—	—	—
273	—	—	—	—	—	—

been identified in our DFT calculations. VDE, E_b, the magnetic moments, vibrational frequencies, as well as the HOMO–LUMO gaps have also been calculated for these structures. The stability and dependence of these properties on the cluster sizes have been analyzed. The geometric structures of these clusters are highly ordered and symmetric. The reduced HOMO–LUMO gap found for $m = 3$ (as shown in Fig. 4) can be explained by the s–d hybridization between rhodium and cobalt atoms[40] as can be seen from Fig. 2 and 3 where the HOMO–LUMO molecular orbital's charge density is shown. The magnetic moment is prominently enhanced in rhodium/cobalt alloy (mixed) clusters. This may be attributed to charge transfer and therefore to exchange spin splitting in atomic clusters. The present results have shown that small rhodium/cobalt clusters are magnetic and that they exhibit significantly larger magnetic moments than corresponding bulk materials. Moreover, the magnetic moments found at the cobalt atoms seem to be relatively independent of the rhodium concentration, although the presence of a cobalt atom as an impurity in rhodium clusters seems to increase the local magnetic moments found in its rhodium neighboring atoms. The observed enhancements in cluster magnetism due to the presence of a cobalt atom may also have the effect of increasing the relative stability of the alloyed cluster. It would be interesting to extend the systems under current investigation to larger sizes, and experimental and theoretical investigations in this direction are in progress.

Acknowledgements

MRB and LGG acknowledge support from PAPIIT IN120109, UNAM project, and from DGSCA UNAM. The calculations were performed on the computational equipment at the supercomputer Kan-Balam, and the cluster computing facility at HRI (http://cluster.hri.res.in). LGG acknowledges support from CONACYT (financial support No 227089), and to the IIM (Instituto de Investigaciones en Materiales) for the use of its facilities. KHB thanks the Division of Materials Sciences and Engineering, Office of Basic Energy Sciences, U.S. Department of Energy, for support of this work under Grant Number DE-FG02-09ER46558.

References

1 J. L. Elkind, F. D. Weiss, J. M. Alford, R. T. Laaksonen and R. E. Smalley, *J. Chem. Phys.*, 1998, **88**, 5215.
2 Y. M. Hamrick and M. D. Morse, *J. Phys. Chem.*, 1989, **93**, 6494.
3 C. Adlhart and E. Uggerud, *J. Chem. Phys.*, 2005, **123**, 214709.
4 D. Harding, M. S. Ford, T. R. Walsh and S. R. Mackenzie, *Phys. Chem. Chem. Phys.*, 2007, **9**, 2130.
5 M. S. Ford, M. L. Anderson, M. P. Barrow, D. P. Woodruff, T. Drewello, P. J. Derrick and S. R. Mackenzie, *Phys. Chem. Chem. Phys.*, 2005, **7**, 975.
6 M. B. Knickelbein and S. Yang, *J. Chem. Phys.*, 1990, **93**, 1476.
7 M. B. Knickelbein and S. Yang, *J. Chem. Phys.*, 1990, **93**, 5760.
8 H. Grönbeck, A. Rosén and W. Andreoni, *Phys. Rev. A: At., Mol., Opt. Phys.*, 1998, **58**, 4630.
9 Y.-C. Bae, H. Osanai, V. Kumar and Y. Kawazoe, *Phys. Rev. B: Condens. Matter Mater. Phys.*, 2004, **70**, 195413.
10 T. R. Walsh, *J. Chem. Phys.*, 2006, **124**, 204317.
11 D. Harding, S. R. Mackenzie and T. R. Walsh, *J. Phys. Chem. B*, 2006, **110**, 18272.
12 M. Respaud, J. M. Broto, H. Rakoto, A. R. Fert, L. Thomas, B. Barbara, M. Verelst, E. Snoech, P. Lecante, A. Mosset, J. Osuna, T. Ould Ely, C. Amiens and B. Chaudret, *Phys. Rev. B: Condens. Matter*, 1998, **57**, 2925.
13 M. C. Fromen, J. Morillo, M. J. Casanove and P. Lecante, *Europhys. Lett.*, 2006, **73**, 885.
14 J. Guevara, A. M. Llois, F. Aguilera-Granja and J. M. Montejano-Carrizales, *Solid State Commun.*, 1999, **111**, 335.
15 X. Xu, S. Yin, R. Moro and W. A. de Heer, *Phys. Rev. Lett.*, 2005, **95**, 237209.
16 Q.-M. Ma, Z. Xie, J. Wang, Y. Liu and Y.-C. Li, *Phys. Lett. A*, 2006, **358**, 289.
17 J. P. K. Doye and D. J. Wales, *J. Phys. B: At., Mol. Opt. Phys.*, 1996, **29**, 4859.
18 M. C. Fromen, A. Serres, D. Zitoun, M. Respaud, C. Amiens, B. Chaudret, P. Lecante and M. J. Casanove, *J. Magn. Magn. Mater.*, 2002, **242–245**, 610.
19 S. Dennler1, J. Morillo and G. M. Pastor, *J. Phys.: Condens. Matter*, 2004, **16**, S2263.
20 H. Cantera-López, J. M. Montejano-Carrizales, F. Aguilera-Granja and J. L. Morán-Lápez, *Eur. Phys. J. D*, 2010, **57**, 61.
21 N. Shen, J. Wang and L. Zhu, *Chem. Phys. Lett.*, 2008, **467**, 114.
22 T. Sondón, A. Saúl and J. Guevara, *Phys. B*, 2007, **398**, 352.
23 G. Moraïtis, H. Dreyssé and M. A. Khan, *Phys. Rev. B: Condens. Matter*, 1996, **54**, 10.
24 S. Dennler, J. Morillo and G. M. Pastor, *Surf. Sci.*, 2003, **532**, 334.
25 P. Hohenberg and W. Kohn, *Phys. Rev.*, 1964, **136**, B864.
26 S. N. Khanna and P. Jena, *Chem. Phys. Lett.*, 2001, **336**, 467.
27 S. N. Khanna, M. R. Beltrán and P. Jena, *Phys. Rev. B: Condens. Matter*, 2001, **64**, 235419.
28 N. O. Jones, S. N. Khanna, T. Baruah, M. R. Pederson, W.-J. Zheng, J. M. Nilles and K. H. Bowen, *Phys. Rev. B: Condens. Matter Mater. Phys.*, 2004, **70**, 134422.
29 J. Lv, F.-Q. Zhang, X.-H. Xu and H.-S. Wu, *Chem. Phys.*, 2009, **363**, 65.
30 M. Gerhards, O. C. Thomas, J. M. Nilles, W.-J. Zheng and K. H. Bowen, *J. Chem. Phys.*, 2002, **116**, 10247.

31 J. P. Perdew, K. Burke and M. Ernzerhof, *Phys. Rev. Lett.*, 1996, **77**, 3865.
32 N. Godbout, D. R. Salahub, J. Andzelm and E. Wimmer, *Can. J. Chem.*, 1992, **70**, 560.
33 J. U. Reveles and A. M. Köster, *J. Comput. Chem.*, 2004, **25**, 1109.
34 A. M. Köster, R. Flores-Moreno and J. U. Reveles, *J. Chem. Phys.*, 2004, **121**, 681.
35 B. I. Dunlap, J. W. D. Connolly and J. R. Sabin, *J. Chem. Phys.*, 1979, **71**, 4993.
36 W. Mintmire and B. I. Dunlap, *Phys. Rev. A: At., Mol., Opt. Phys.*, 1982, **25**, 88.
37 P. Calaminici, F. Janetzko, A. M. Köster, R. Mejia-Olvera and B. Zuñiga-Gutierrez, *J. Chem. Phys.*, 2007, **126**, 044108.
38 A. M. Köster, P. Calaminici, R. Flores-Moreno, G. Geudtner, A. Goursot, T. Heine, F. Janetzko, S. Patchkovski, J. U. Reveles, A. Vela and D. R. Salahub, *deMon2k*, deMon developers, 2004.
39 N. O. Jones, M. R. Beltrán, S. N. Khanna, T. Baruah and M. R. Pederson, *Phys. Rev. B: Condens. Matter Mater. Phys.*, 2004, **70**, 165406–7.
40 A. J. Cox, J. G. Louderback and L. A. Bloomfield, *Phys. Rev. Lett.*, 1993, **71**, 923.